Impact of GEM foil hole geometry on GEM detector gain

2015 JINST 10 P12014

(http://iopscience.iop.org/1748-0221/10/12/P12014)

Jinst

Published by IOP Publishing for Sissa Medialab

Received: *October 16, 2015*
Accepted: *November 15, 2015*
Published: *December 18, 2015*

Impact of GEM foil hole geometry on GEM detector gain

A. Karadzhinova,[a,1] **A. Nolvi,**[b] **R. Veenhof,**[c,d] **E. Tuominen,**[a] **E. Hæggström**[b] **and I. Kassamakov**[a,b]

[a] *Detector Laboratory, Helsinki Institute of Physics, P.O. Box 64, 00014, Helsinki, Finland*
[b] *Department of Physics, University of Helsinki, P.O. Box 64, 00014, Helsinki, Finland*
[c] *Department of Physics, Uludağ University, 16059 Bursa, Turkey*
[d] *RD51 collaboration, CERN, 1211Genève 23, Switzerland*

E-mail: aneliya.karadzhinova@helsinki.fi

Abstract: Detailed 3D imaging of Gas Electron Multiplier (GEM) foil hole geometry was realized. Scanning White Light Interferometry was used to examine six topological parameters of GEM foil holes from both sides of the foil. To study the effect of the hole geometry on detector gain, the ANSYS and Garfield ++ software were employed to simulate the GEM detector gain on the basis of SWLI data. In particular, the effective gain in a GEM foil with equally shaped holes was studied. The real GEM foil holes exhibited a 4% lower effective gain and 6% more electrons produced near the exit electrode of the GEM foil than the design anticipated. Our results indicate that the GEM foil hole geometry affects the gain performance of GEM detectors.

Keywords: Control and monitor systems online; Detector modelling and simulations II (electric fields, charge transport, multiplication and induction, pulse formation, electron emission, etc); Micropattern gaseous detectors (MSGC, GEM, THGEM, RETHGEM, MHSP, MICROPIC, MICROMEGAS, InGrid, etc); Detection of defects

[1] Corresponding author.

doi:10.1088/1748-0221/10/12/P12014

2015 JINST 10 P12014

Contents

2015 JINST 10 P12014

1 Introduction

Gas Electron Multiplier (GEM) detectors are radiation detectors [1] used in high-energy physics and in nuclear physics experiments. The active GEM element is a thin (approximately 50 ± 1 μm) polyimide foil with a 5 ± 1 μm copper/chromium coating on both sides [2]; see figure 1.

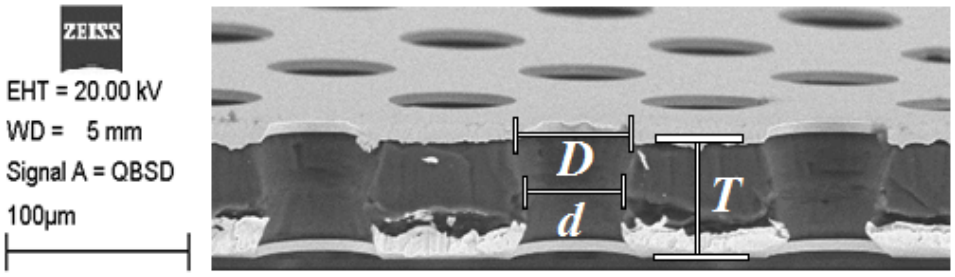

Figure 1. Cross-section of GEM foil obtained with a Scanning Electron Microscope. The outer *diameter* (D) and inner *diameter* (d) of the holes, as well as the foil *thickness* (T), are indicated.

The foils have hourglass-shaped holes etched through them using lithography. Typically, their outer *diameter D* is 70 ± 5 μm, the inner *diameter d* is 50 ± 5 μm, and the hole pitch *P* is 140 μm [2]. Local variations in the size, shape [3], and rim roughness of the holes can alter the operational characteristics of the GEM foil. Consequently, these parameters should be uniform to achieve even performance across the active surface of the detector. There are approximately 6400 holes per cm^2 of GEM foil.

Several techniques are used for GEM quality assurance (QA). Most often a high-voltage test is applied — leakage current measurement of the GEM foil [4]. Optical/visual QA of GEM foils is less common. There are also ideas for X-ray-based GEM foil inspection.

Visual QA is necessary not only to examine the size and the shape of the hole, but also to catch foil defects, residuals, and dust. Visual inspection is the only way to confirm the hole parameters. Tardiness is the main disadvantage of visual QA compared to HV QA. Visual inspection usually takes hours, while the HV test is done in approximately 30 min. This drawback is pronounced since there is a need for large-area GEM foil detectors.

The optical scanning system (OSS) for the quality assurance of GEM foils was developed in the Laboratory for Nuclear Science at the Massachusetts Institute of Technologies (U.S.A.) in 2006 [5, 6]. The University of Helsinki (Finland) [7] and Temple University (Philadelphia, U.S.A.) [8] developed their own systems on the basis of the first one.

Previously, we have calibrated our large-area OSS for quality assurance of GEM foils by using a transfer standard specifically manufactured for this purpose [9, 10]. The correlation between the GEM hole size distribution and the corresponding gain variation has also been studied [11].

2 Methods

The major advance represented by the current study is the use of a 3D reference device to reveal the GEM foil hole geometry; see figure 2. In addition to the parameters used nowadays, we introduce and study four new parameters — the *shift* (S) between the centers of the inner and outer diameters, the total foil *thickness* (T), and metal (T_m) and polyimide (T_p) *thickness* — that we propose should be controlled during GEM foil manufacturing. The variations in the pitch and rim roughness parameters were not studied in this research.

A customized GEM foil sample allowed us to study the variation in hole size, as well as concentricity issues between the inner *diameter d* and outer *diameter D* of the holes. The ± 5 nm vertical resolution of our Scanning White Light Interferometer (SWLI) [12] permitted for the first time the study of variation in the foil *thickness* as a basis for detailed 3D QA analysis of the GEM foil hole geometry.

The effects of the six (d, D, S, T, T_m, T_p) parameters were examined using the ANSYS [13] computer-aided engineering software and the Garfield++ [14] toolkit for detailed simulation of particle detectors. We used ANSYS to create a field calculation for the GEM foil hole, using topological parameter values obtained by SWLI. Garfield++ was then used to simulate the detector gain for the real geometry of the hole. 1000 avalanches in an $ArCO_2$ 70/30% gas mixture with a penning factor r_p = 0.7 and V_{GEM} = 600 V were applied to the foil [3]. The probability r_p that an excited Ar atom ionizes a CO_2 molecule through penning transfer was studied [15].

2015 JINST 10 P12014

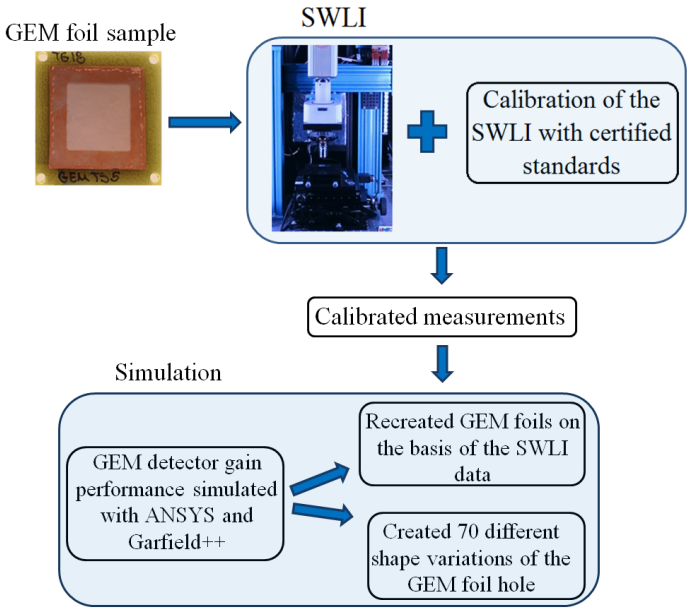

Figure 2. Flow chart illustrating the logic of the study.

2.1 Setup

2.1.1 GEM foil sample preparation

A randomly chosen GEM foil was cut into $2.5 \times 2.5\,\mathrm{cm}^2$ pieces. Using the GEM foil-frame gluing technology [16], these pieces were cleaned and glued to a standard SF4 PCB (polychlorinated biphenyl) frame; see figure 3. This procedure took place in a class 1000 clean room.

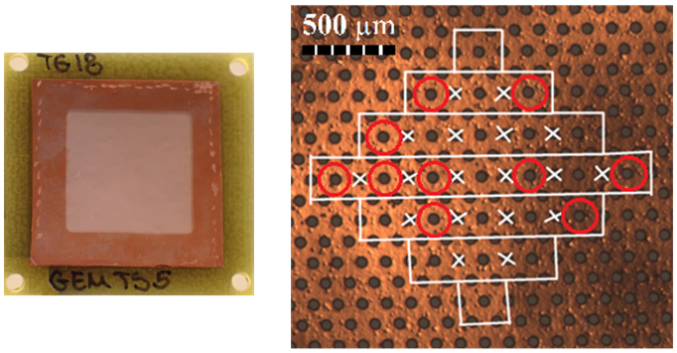

Figure 3. GEM foil $2.5 \times 2.5\,\mathrm{cm}^2$ standard (left). Zoom-in view of the map of the 25 SWLI holes that were examined (right); the red circles show the 10 holes chosen for the simulation studies.

2.1.2 Scanning White Light Interferometry

Our full-field-of-view non-contact SWLI device measures surface topography. On the basis of the reflection from the measured surface of a white light beam into an interferometric objective, this technique provides quantitative information across large areas with ± 5 nm vertical resolution [12].

2015 JINST 10 P12014

Our device had a NIKON CF IC Epi Plan DI 50X 0.55NA objective lens with 25X (0.5X tube-lens NIKON) total magnification, a HAMAMTSU Orca Flash 2.8 camera, and a halogen bulb light source (Philips, type 77241, Amsterdam, The Netherlands).

2.2 SWLI measurements

The six main GEM foil hole parameters were examined with SWLI: d, D, S, T, T_m, and T_p. All 25 holes in our sample were scanned three times from the *top* and *bottom* of the sample without translating the hole between the images. Using the MountainsMap software [17], the GEM foil parameters for each hole were determined from the SWLI data.

The hole *diameters* d and D of the GEM foil sample were defined using a 'contour extraction' method (25 holes × 2 diameters × 2 sides × 3 times = 300 measurements). This method, shown in figure 4, employs the contour extraction feature of MMap. The *top* and *bottom diameters* d and D were then defined by multiplying the radii that had been obtained by two.

During the contour extraction procedure poor concentricity [18] between d and D was observed on both sides of the foil. Concentricity is the common center of cylindrical or spherical parts. We studied the relative *shift* (S) between d and D on the *top* and the *bottom* sides of the GEM foil sample when assuming the center of d to be the reference point for each side. The values were obtained using the distance measure feature of the MMap software; see figure 4 (right). Each value was formed as an average of three measurements (25 holes × 1 shift × 2 sides × 3 times = 150 measurements).

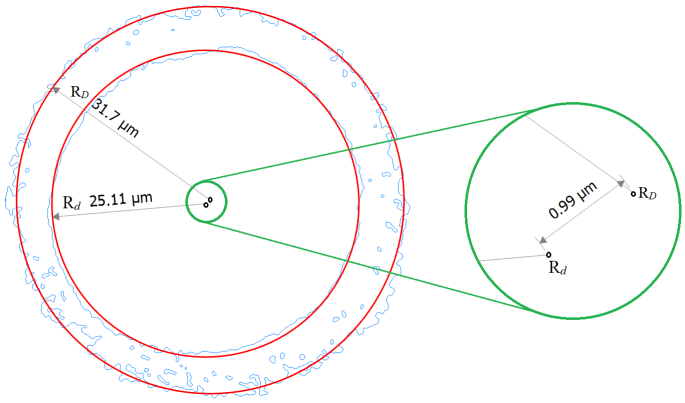

Figure 4. Inner (d) and outer (D) *diameter* extraction by the contour method for SWLI (left). The measured *shift* S between the centers of d and D (right) was 0.99 μm for hole #8.

Detailed 3D QA analysis of the GEM foil hole geometry was performed. The vertical resolution of the SWLI allowed us to examine the foil *thickness* (T) for the first time and study its variation across the sample. Figure 5 shows the total *thickness* of the GEM foil around hole #8 scanned with SWLI.

Figures 4 and 5 indicate the rim roughness R of the inner and outer diameter. The effect of this GEM foil parameter was not studied in the present study.

All T values were measured with SWLI and obtained using the step height ISO 5436 feature of the MMap software. The GEM foil sample was placed and gently pressed onto a flat reference surface (optically flat, with -0.07 μm out-of-flatness and 0.02 μm out-of-parallelism). Each value was calculated as an average of 4 step height profiles for the *top* and the *bottom* side of a single hole

2015 JINST 10 P12014

(25 holes × 1 height × 4 profiles × 2 sides × 3 times= 600 measurements). The same technique was used to obtain the metal and polyimide *thickness* on both sides of the GEM foil sample; see figure 6.

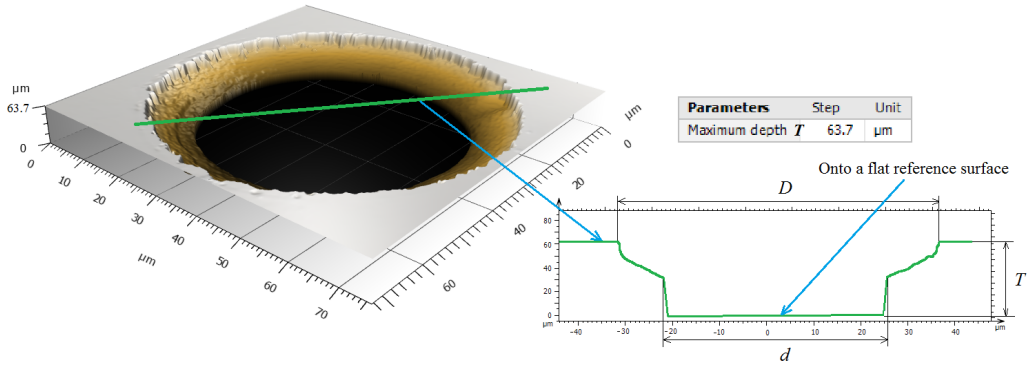

Figure 5. MountainsMap software step height feature used in the study of the total *thickness T* of the GEM foil sample.

The sandwiched polyimide, close to the center of the holes, appears to be very thin and transparent to the SWLI, which left an unknown area in the image. Nevertheless, the measured total *thickness* (63.17 ± 0.07 μm) around hole #8 of our GEM foil sample was close to the nominal value for the GEM foil (60 ± 3 μm). Figure 7 shows a *thickness* reconstruction of GEM foil hole #8.

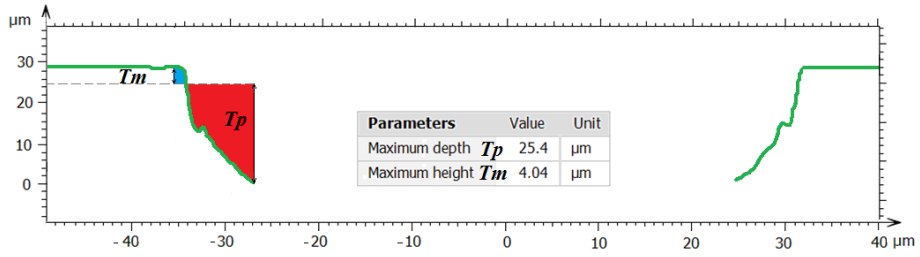

Figure 6. MountainsMap software step height feature used in the metal (T_m) and polyimide (T_p) *thickness* study of the GEM foil sample.

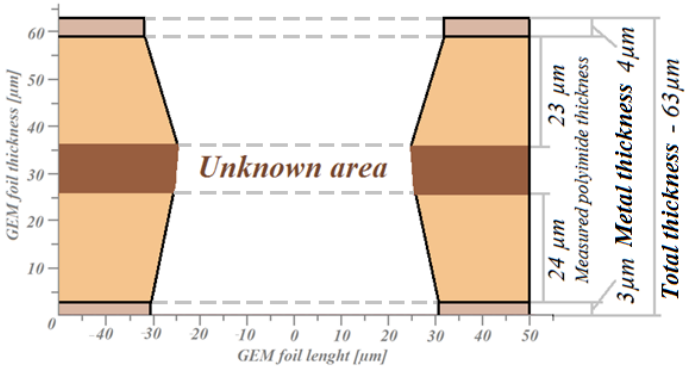

Figure 7. *Thickness* reconstruction of GEM foil hole #8.

2015 JINST 10 P12014

The uncertainty of all the measurements for each hole was defined as required by [19] and [20]. All the SWLI measurements were performed manually, using the same features of MMap. The precision and accuracy of the SWLI measurements depend on identifying the edges of the hole and on the granularity of the computer mouse movement.

2.3 Simulation methods

The ANSYS and Garfield ++ software were employed to study the effective gain as a function of hole parameters in a GEM foil with equally shaped holes. This simulation study focused on an hourglass-shaped hole with a nominal d and D (50 ± 5 μm and 70 ± 5 μm), T of 60 ± 3 μm, and P of 140 μm. We created and studied 70 different shape variations of the GEM foil hole. The five basic scenarios are shown in figure 8.

First, the nominal hourglass hole geometry (#1) was simulated and its effective gain was studied. After that the *top* part of the hole was kept static while the *bottom* part was moved from the center to the left and then from the center to the right with 1 μm steps in a total range of -5 to 5 μm (scenario #2 in figure 8). The same was done for scenario #3, but the *bottom* part of the hole was kept static. In the end, scenarios #4 and #5 were studied when both parts of the hole were moved in opposite directions with 1 μm steps in a total range of -5 to 5 μm.

A study of the effective gain as a function of the measured GEM foil hole shape was also performed. ANSYS was used to recreate the GEM foil on the basis of SWLI data from 10 holes in our GEM foil sample. These 10 holes were randomly chosen from the 25 holes examined with SWLI.

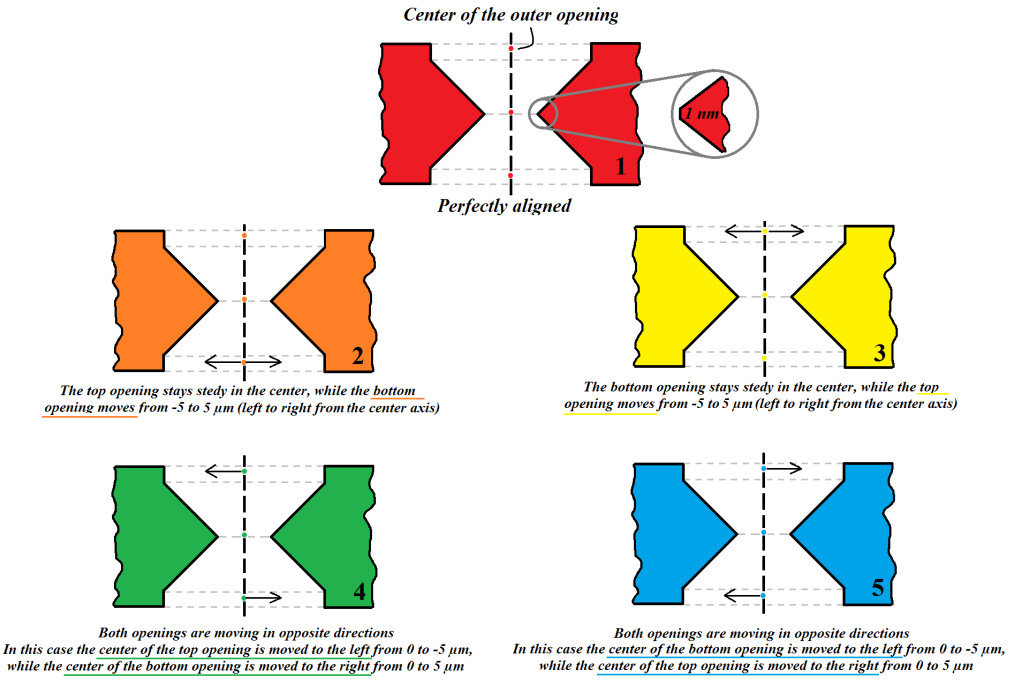

Figure 8. Simplified side view of the five basic scenarios: #1 — original hourglass-shaped hole; #2 — *bottom* opening moves but static *top*; #3 — *top* opening moves but static *bottom*; #4 — *top* to the left and *bottom* to the right; #5 — *top* to the right and *bottom* to the left.

2015 JINST 10 P12014

The 10 holes were divided into three categories: A — deviation in the hole parameters with ±1 μm than the nominal values — see figure 4 and table 1; B — *top* and *bottom* hole elements with a shift of more than 1 μm from the center of the hole; C — with a difference of more than 1 μm between the *top* and *bottom* opening shift. The hole shapes shown in figure 9 present (from left to right) the hourglass-shaped hole with nominal values and the replicated GEM foil holes from categories B and C with their parameter values as measured with SWLI.

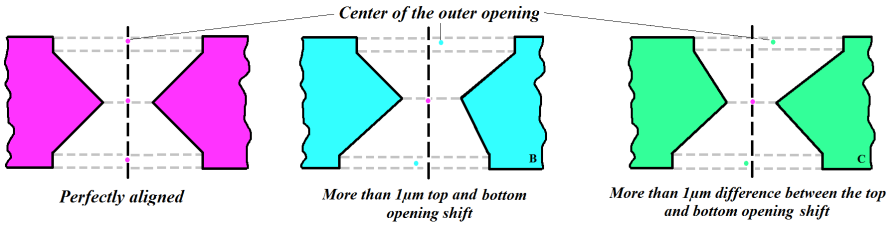

Figure 9. Simplified side view of the B and C GEM foil hole categories. See figure 3 for an A category GEM foil hole.

Next, the performance of the 10 replicated GEM foil holes simulated with Garfield ++ was evaluated against an hourglass-shaped hole (nominal result). The simulation results are reported in the results section.

2.3.1 ANSYS

ANSYS is a computer-aided engineering software program that we used to create a field calculation for a single GEM foil with equally shaped holes. For each simulated GEM hole category, a foil sandwich structure (thin polyimide foil with metal coating on both sides) surrounded by a gas mixture was created; see figure 10 (left).

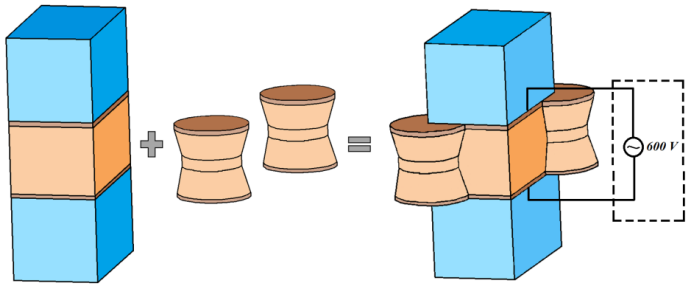

Figure 10. Side view of the GEM foil sandwich structure (polyimide in beige and metal in brown) and gas mixture (in blue) created using ANSYS.

The hole shape — see figure 10 (middle) — was created from three polyimide layers and two layers of metal; see figure 7. All the volumes were then meshed to create a single body — see figure 10 (right) — which was later cut out of the initial sandwich structure to achieve the final GEM foil lookalike; see figure 11 (middle). V_{GEM} = 600 V was applied to the simulated foil and a field calculation was performed for all 10 measured GEM foil holes and the 70 hole shaping scenarios.

2015 JINST 10 P12014

2.3.2 Garfield ++

Garfield ++ is a toolkit for the detailed simulation of particle detectors. Garfield ++ was employed to simulate the detector gain using the ANSYS field calculations as input. For each of the 10 GEM holes and the 70 scenarios, a Garfield ++ simulation was performed for 1000 avalanches in an $ArCO_2$ 70/30% gas mixture, a penning factor r_p = 0.7, and V_{GEM} = 600 V applied to the foil.

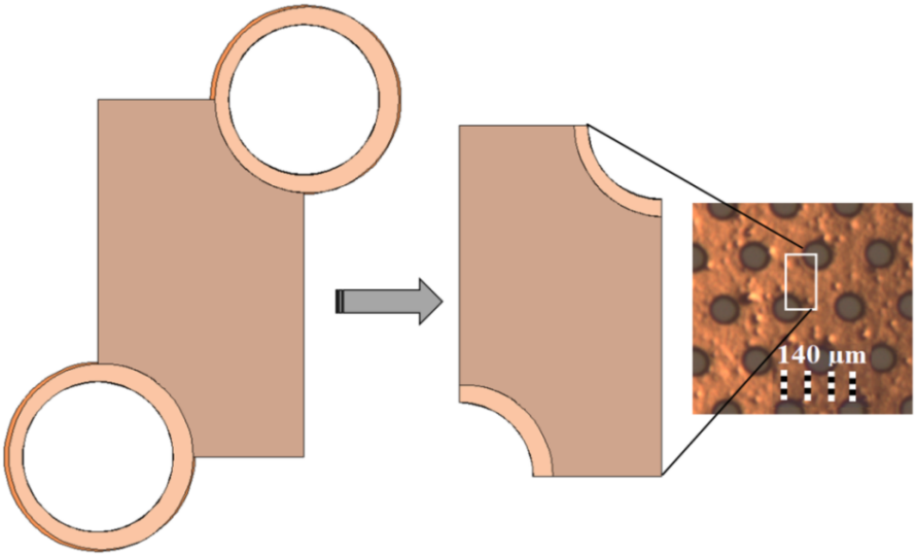

Figure 11. Top view of GEM foil holes created with ANSYS. The part in the center represents a small piece of a real GEM foil, equal to the area inside the white rectangle.

3 Results

3.1 GEM foil hole parameters examined with SWLI

Figure 12 illustrates the GEM foil sample hole #8, scanned by SWLI and compared with the corresponding OSS image. A contour extraction method was used for both hole *diameters*, d and D; see figure 4.

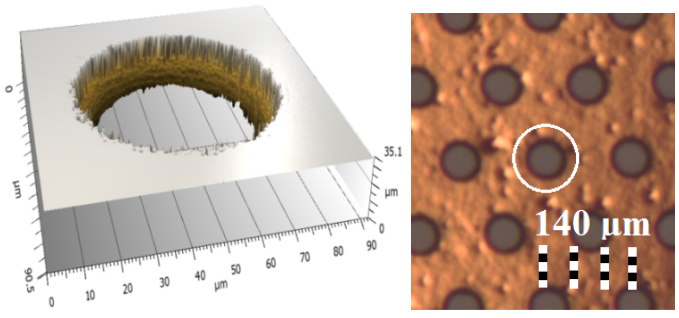

Figure 12. GEM foil sample hole #8 *diameter* imaged with SWLI (left) and OSS (right).

The extraction method confirmed the observed *shift S* between the centers of the *top* and *bottom* holes determined by SWLI; see figure 4 (right). It was, as expected, also possible to determine the

2015 JINST 10 P12014

total foil *thickness* T, as well as the *thickness* of the metal T_m and polyimide layers T_p. Table 1 presents the *top* and *bottom* parameters obtained for GEM foil sample hole #8. The results of the GEM foil sample that was examined indicated a probable mask misalignment during the fabrication.

Table 1. SWLI measured *top* and *bottom* parameters of GEM foil hole #8 with total *thickness* T of 63.17 ± 0.07 μm. The errors presented have a coverage factor k = 2.

Feature	***Top***	***Bottom***
d	51.18 ± 0.28 μm	51.16± 0 04 μm
D	62.81 ± 0.37 μm	63.15± 0.11 μm
S	0.22 ± 0 07 μm	1.41 ± 0 14 μm
T_m	3.64 ± 0.55 μm	3.28 ± 0.42 μm
T_p	22.96 ± 1.01 μm	23.35 ± 0.75 μm

Figure 13 shows a comparison of the *shift* between d and D on the *top* and *bottom* sides measured with SWLI for the 25 holes of the GEM foil sample. The plot indicates that holes #5 and #22 feature a relative *top* and *bottom* side *shift* of 3 μm. The impact of such a big shift is presented in the simulation section below.

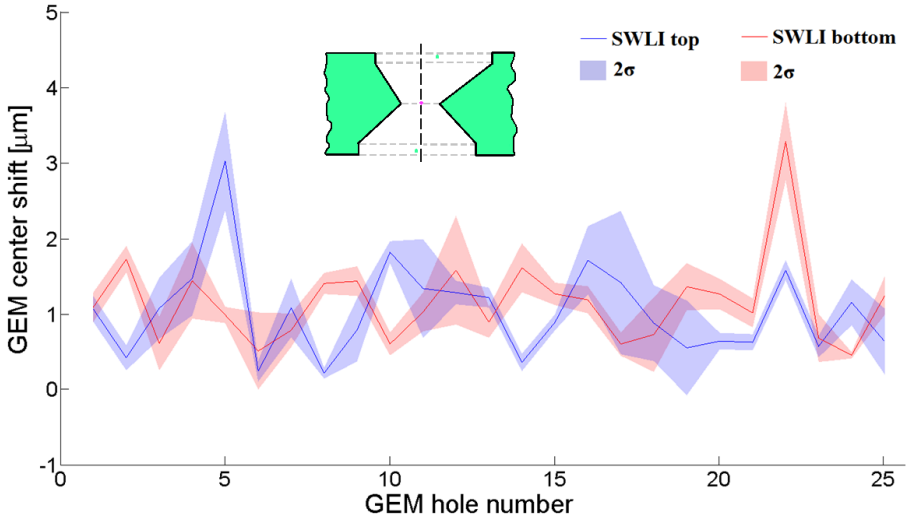

Figure 13. SWLI comparison of the *shift* between d and D on the *top* and *bottom* side (see figure 9 (right)) for the 25 holes in the GEM foil sample.

Figure 14 shows the total *thickness* (T) measured with SWLI for the 25 holes of the GEM foil. The T values ranged from 62.30 to 65.60 μm. The *thickness* of the GEM foil close to most of the holes that were examined was 5.6 μm larger than the nominal thickness (60 ± 3 μm).

3.2 Comparison of multiple holes

This section focuses on the variation in the *diameter* of the holes located in one compact area of the GEM foil sample; see figure 3. This data was obtained by the contour extraction method (figure 4). Figure 15 presents a comparison of multiple holes for the *top* and *bottom* d measured with SWLI

2015 JINST 10 P12014

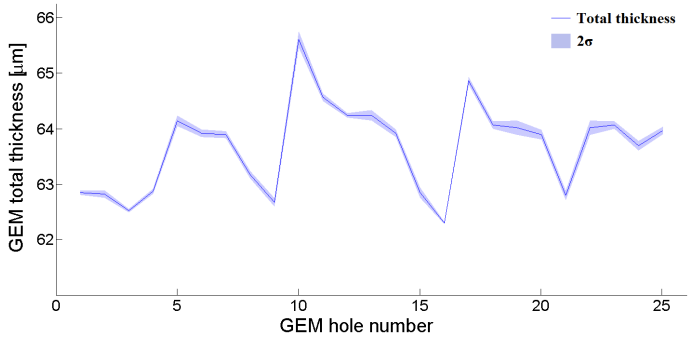

Figure 14. SWLI results for total foil *thickness* (T) (see figure 5) around the 25 holes in the GEM foil sample.

for all 25 holes from the GEM sample, whereas figure 16 presents the same comparison but for the *top* and *bottom* D.

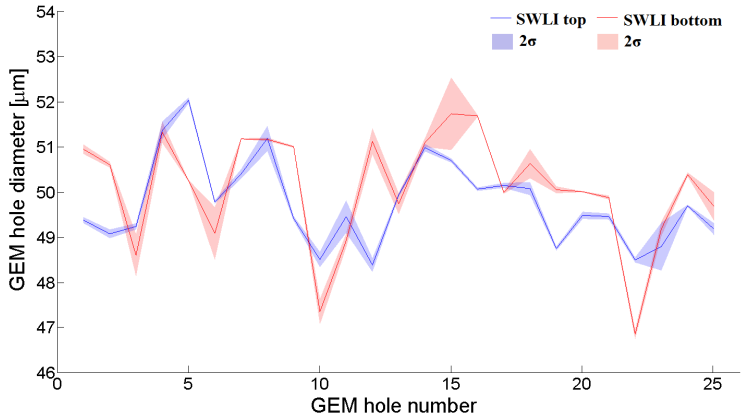

Figure 15. The 25 inner holes d (see figure 4) in the GEM foil sample measured with SWLI.

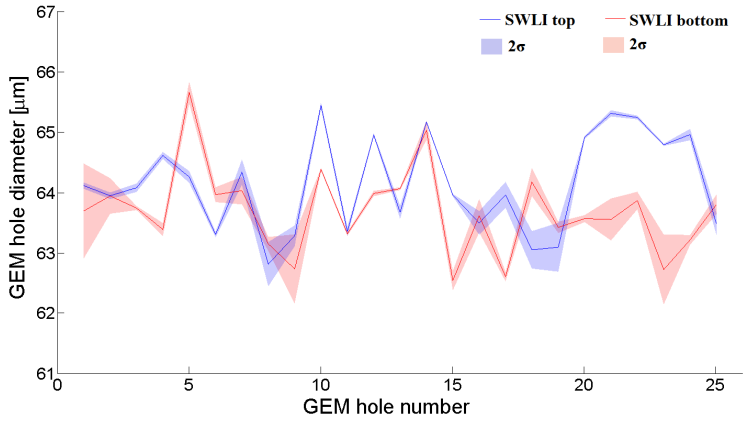

Figure 16. The 25 outer holes D (see figure 4) in the GEM foil sample measured with SWLI.

Although there was fluctuation in the *top* and *bottom* d values, they all agree with the nominal

2015 JINST 10 P12014

value for the GEM foil, with a typical d of 50 ± 5 μm. However, the values obtained for D are much smaller (-7.5 μm for both the *top* and *bottom* sides) than the nominal value (70 ± 5 μm). All the data that was collected can be found in Supplementary_Material.doc (online resource 1).

3.3 Simulations

Figure 17 presents the variation in the effective gain studied with Garfield ++ for different shapes of a single hole in a GEM foil with equally shaped holes. A 7% drop in the effective gain was observed compared to the effective gain of the nominal hourglass-shaped hole. Figure 18 shows that the electrons produced near the exit electrode that do not contribute to the effective gain. A 7% maximum increase was observed in this region of the foil.

During the GEM hole parameter extraction values different from the nominal ones were observed for the *top* and *bottom* sides of the foil. 10 of the 25 holes from our GEM foil sample were randomly chosen to be recreated, as a single foil, with ANSYS and their gain was studied with Garfield ++.

Figure 19 illustrates the simulated effective gain (left) compared to that of the nominal hourglass-shaped hole foil and the electrons produced near the exit electrode for 10 real GEM foil hole geometries.

Several of the real GEM hole geometries exhibited a 4% lower effective gain compared to the nominal case. A close look at the hole geometry shows that the high slope from the center to the *bottom* of the foil might be the reason for this phenomenon. 6% more electrons were produced near the exit electrode of the GEM foil, compared to the nominal case.

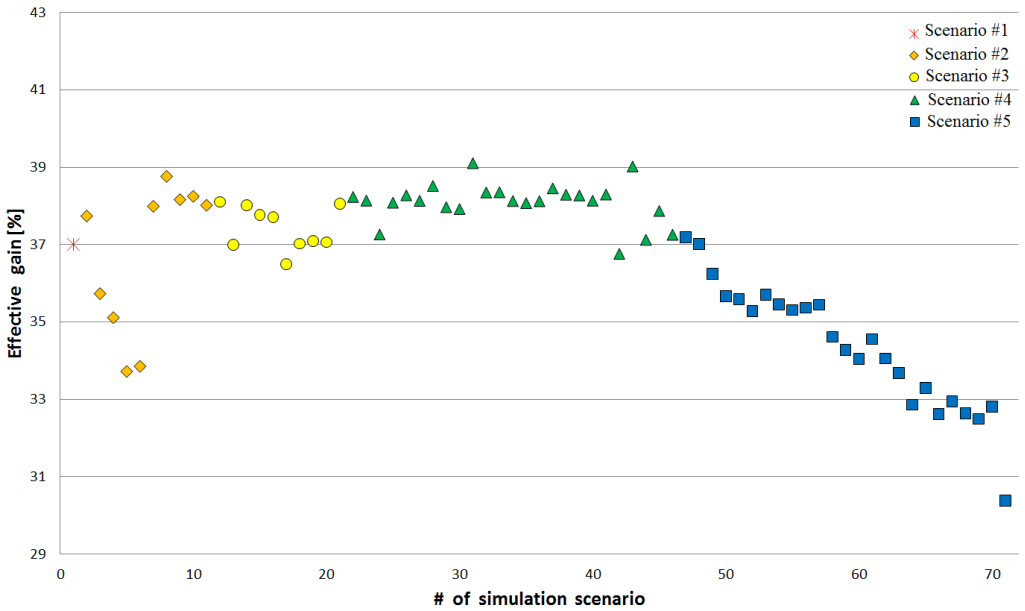

Figure 17. Simulated effective gain of the GEM foil hole with 70 differently shaped scenarios compared to the nominal hourglass-shaped hole. See figure 8 for the color codes.

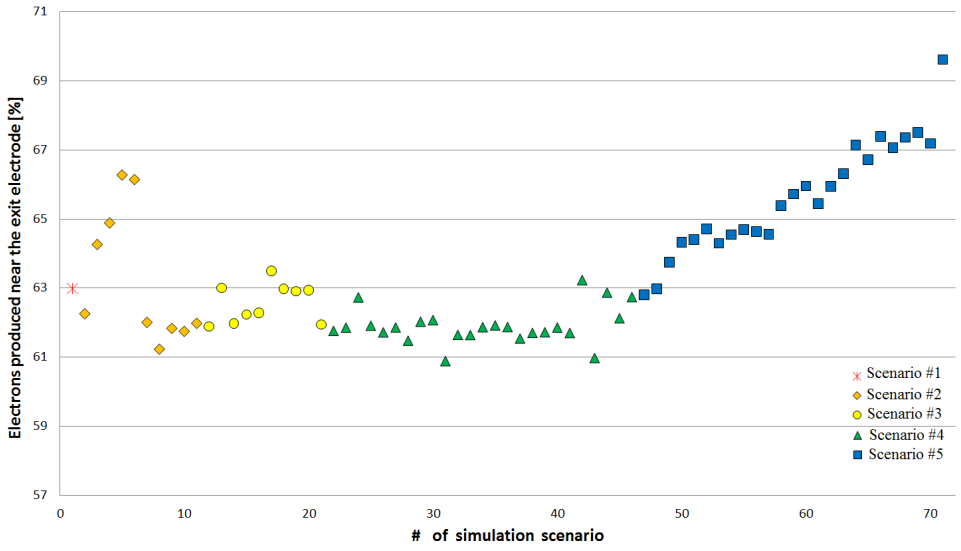

Figure 18. Electrons produced near the exit electrode of the GEM foil for 70 differently shaped scenarios compared to the situation in the nominal hourglass-shaped hole. See figure 8 for the color codes.

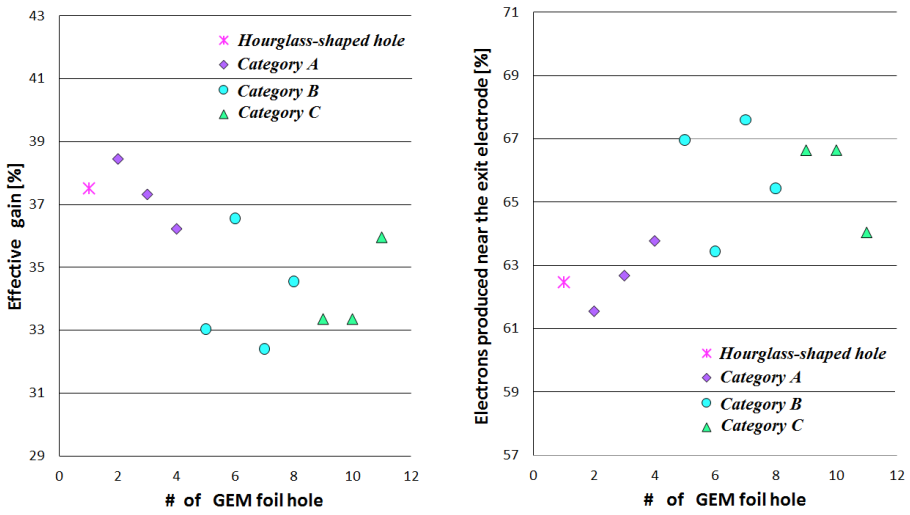

Figure 19. Simulated results based on 10 SWLI measured GEM foil hole geometries. The magenta marker is for the hourglass-shaped hole and purple, cyan, and green are for the A (see figure 4), B, and C categories (see figure 9), respectively.

4 Discussion

There are no detailed studies in the literature on the shape and size of GEM foil holes. Hitherto the holes have been assumed to be perfectly hourglass-shaped [3] and only nominal hole shapes have been simulated [21]. There are papers reporting on both simulations and real measurements with regard to the optimal hole size for high gain [3, 22], and [23]. In these cases all the holes were assumed to be identical. Most previous research on detector gain focuses on the gas mixture and pressure and the voltage applied rather than the actual hole shape [15, 24], and [25].

2015 JINST 10 P12014

In the current study we used a calibration sample (to confirm the tool calibration) with a surface comparable to that of the GEM foil to obtain accurate values for the real-life GEM foil hole geometry. To guarantee accurate and traceable results we ensured that both individual holes and ensembles of holes were correctly imaged. This was done by collecting the data with a calibrated SWLI device. This kind of study has not been performed before. We also proposed a new approach to the 3D quality assurance analysis of GEM foil hole geometry. This method applied to a double masked GEM foil employs six parameters: inner (d) and outer (D) hole *diameter*, *shift* (S) between the centers of the two holes, and the total foil (T), metal (T_m), and polyimide layer (T_p) *thicknesses*.

The S parameter is, however, a little tricky. How does one know which side has moved? The GEM foil fabrication process starts with etching from the *top* and then from the *bottom* to the center of the foil. Hence the *top* side pitch is the first parameter to be created. It is therefore possible to have misalignment of both *top* and *bottom* pitches. However, in this study we are observing a *shift* between D and d on both sides, which should be due to the etching process — the etchant does not create a perfectly centered cone. Consequently our approach of using the *top* hole center as our reference point should be solid.

To determine the effect of hole geometry on gain, the ANSYS and Garfield ++ softwares were employed to simulate the GEM detector gain performance on the basis of measured SWLI data. The effective gain in a single foil with equally shaped holes was also studied. Compared to predictions based on the ideal geometry, the hole based on the measured geometry featured 4% lower gain and 6% more produced electrons near the exit electrode of the GEM foil. Our results prove that the hole geometry affects the gain performance of the GEM detectors. The recorded effect, while small, may be important since the simulated cases are ideal — equally shaped holes along the GEM foil. As demonstrated in this study, the GEM foil contains holes of different shapes and sizes. Most papers report that GEM detectors are robust and can tolerate the radiation dose foreseen in 10 years of operation without loss in gain and energy resolution. For instance, LHCb published a paper in 2012 stating that 'as of today we don't observe classical aging effects on our GEM detectors' [26].

The simulations assumed a certain size and shape for all the holes in a GEM foil. For instance, each marker in figure 19 represents a foil with identical holes. A GEM detector gain evaluation on the device level could be performed for an assembly of differently shaped and sized holes over several GEM foil detectors. It is likely that the effective gain could significantly increase or decrease if a foil with different shapes and size holes is simulated. This is future work. The effect of the rim roughness also needs to be examined since asperities concentrate the electric field.

The proposed method is slow if used to examine a GEM foil sized 10 by 10 cm^2. However, knowing the real hole geometry could help improve GEM fabrication, which could lead to better detector performance. Improving GEM foil fabrication is important because it is assumed on the basis of [3–8] that the characteristics of GEM foils strongly affect the behavior of the GEM foil detector.

The present work is important to the field of metrology, as well as for the QA and fabrication of GEM detectors. The study shows that the real GEM hole geometry differs from the designed geometry. It might also provide a deeper understanding of the processes inside the GEM detector during operation. We therefore recommend these parameters to be considered during further development, manufacturing, and performance simulations of GEM foils.

2015 JINST 10 P12014

5 Conclusions

A GEM foil sample and high-resolution SWLI were used for a detailed examination of the geometry of GEM foil holes. Both sides of the sample were examined and six topological foil parameters were determined. On the basis of the measured data, ANSYS and Garfield ++ simulations were performed to study the effect of hole geometry on detector gain. Our results indicated that the real GEM foil holes exhibited a 4% lower effective gain and 6% more electrons produced near the exit electrode of the GEM foil than the design anticipated.

Acknowledgments

This work was partly supported by the EMRP NEW08 MetNEMS project and an associate research excellence grant, NEW08-REG3. The EMRP is jointly funded by the participating countries in the EMRP within EURAMET and the European Union.

We thank Dr. Alessandro Amato and Dr. Francesco Devoto for their C++ and ROOT support.

References

[1] F. Sauli, *GEM: A new concept for electron amplification in gas detectors*, *Nucl. Instrum. Meth.* **A 386** (1997) 531.

[2] R. Oliveira, *MPGDs & GEM foils and detector fabrication techniques*, talk given at the *IWAD and the 14th RD51 Collaboration Meeting*, Kolkata, India, 27–31 Oct 2014.

[3] S. Bachmann, A. Bressan, L. Ropelewski, F. Sauli, A. Sharma and D. Mormann, *Charge amplification and transfer processes in the gas electron multiplier*, *Nucl. Instrum. Meth.* **A 438** (1999) 376.

[4] M. Posik and B. Surrow, *Optical and electrical performance of commercially manufactured large GEM foils*, *Nucl. Instrum. Meth.* **A 802** (2015) 10.

[5] U. Becker, B. Tamm and S. Hertel, *Test and evaluation of new GEMs with an automatic scanner*, *Nucl. Instrum. Meth.* **A 556** (2006) 527.

[6] F. Simon et al., *Development of tracking detectors with industrially produced GEM foils*, *IEEE Trans. Nucl. Sci.* **54** (2007) 2646 [arXiv:0707.2543].

[7] M. Kalliokoski et al., *Study of GEM-Foil Defects with Optical Scanning*, *IEEE Nucl. Sci. Symp. Conf. Rec.*, IEEE (2010), pp. 1446–1449.

[8] M. Posik and B. Surrow, *Research and development of commercially manufactured large GEM foils*, in proceedings of 4$^{\text{th}}$ *Joint Meeting of the APS Division of Nuclear Physics and the Physical Society of Japan*, *Bulletin of the American Physical Society* **59** (2014).

[9] A. Karadzhinova et al., *Calibrating an optical scanner for quality assurance of large area radiation detectors*, *Measur. Sci. Tech.* **25** (2014) 115403.

[10] A. Karadzhinova et al., *Microfabrication of Transfer Standards for Calibration of Optical Quality Assurance System*, in proceedings of *24th Micromechanics and Microsystems Europe Conference*, Espoo, Finland (2013).

[11] T. Hildén et al., *Optical quality assurance of GEM foils*, *Nucl. Instrum. Meth.* **A 770** (2014) 113.

[12] J. Seppä et al., *Quasidynamic calibration of stroboscopic scanning white light interferometer with a transfer standard*, *Opt. Eng.* **52** (2013) 12.

2015 JINST 10 P12014

[13] ANSYS Inc., Southpointe, 2600 ANSYS Drive, Canonsburg, PA 15317, U.S.A. http://www.ansys.com/.

[14] H. Schindler and R. Veenhof, *Garfield++: Simulation of tracking detectors*, http://cern.ch/garfieldpp.

[15] Ö. Şahin et al., *Penning transfer in argon-based gas mixtures*, 2010 *JINST* **5** P05002.

[16] S. Bachmann et al., *Performance of GEM detectors in high intensity particle beams*, *Nucl. Instrum. Meth.* **A 470** (2001) 548.

[17] Digital Surf Inc., 25000 Besançon, France, http://www.digitalsurf.fr/en/index.html.

[18] ISO 1101, *Geometrical product specifications (GPS) — Geometrical tolerancing — Tolerances of form, orientation, location and run-out*, 3rd edition, Geneva, Switzerland (2012).

[19] Joint Committee for Guides in Metrology, *Evaluation of measurement data — Guide to the expression of uncertainty in measurement (GUM)*, JCGM 100:2008.

[20] G. Rodger, *Dimensional Measurement using Vision Systems, Measurement Good Practice Guide No. 39*, National Physical Laboratory, Teddington, U.K. (2010).

[21] G. Bencivenni et al., *A comparison between GEM-based detector simulation and experimental measurements*, *Nucl. Instrum. Meth.* **A 494** (2002) 233.

[22] O. Buyanov, M. Buyanov, R. Orava and V. Tikhonov, *Foil geometry effects on GEM characteristics*, *Nucl. Instrum. Meth.* **A 458** (2001) 698.

[23] F. Sauli, *The gas electron multiplier (GEM): Operating principles and applications*, *Nucl. Instrum. Meth.* **A 805** (2016) 2.

[24] A. Bondar, A. Buzulutskov and L.I. Shekhtman, *High pressure operation of the triple-GEM detector in pure Ne, Ar and Xe*, *Nucl. Instrum. Meth.* **A 481** (2002) 200 [physics/0103082].

[25] F.D. Amaro et al., *Operation of a single-GEM in noble gases at high pressures*, *Nucl. Instrum. Meth.* **A 579** (2007) 62.

[26] A. Cardini et al., *The Operational Experience of the Triple-GEM Detectors of the LHCb Muon System: Summary of 2 Years of Data Taking*, *IEEE Nucl. Sci. Symp. Conf. Rec.*, IEEE (2012), pp. 759–762.

2015 JINST 10 P12014